PROGRESS AND CHALLENGES WITH PEROVSKITE MATERIALS AND DEVICES

Comparison of Ferroelectric Photovoltaic Performance in BFO/BTO Multilayer Thin Film Structure Fabricated Using CSD & PLD Techniques

SAVITA SHARMA,[1,5] ANJALI SHARMA,[2] VINAY GUPTA,[1] NITIN K. PURI,[3] and MONIKA TOMAR [4,6]

1.—Department of Physics and Astrophysics, University of Delhi, Delhi, India. 2.—Physics Department, Atma Ram Sanatan Dharma College, University of Delhi, Delhi, India. 3.—Department of Applied Physics, Delhi Technological University, Delhi, India. 4.—Physics Department, Miranda House, University of Delhi, Delhi, India. 5.—Physics Department, Kalindi College, University of Delhi, Delhi, India. 6.—e-mail: monikatomar@gmail.com

Multilayer thin film structures of BFO/BTO possessing a distinct count of layers were prepared by chemical solution deposition and pulsed laser deposition techniques. These two different deposition techniques have been explored to investigate the effect of deposition technique on ferroelectric-photovoltaic properties of the BFO/BTO system in detail. Multilayers prepared using both the techniques exhibit pure perovskite structure showing the tetragonal and rhombohedral phases of BTO/BFO respectively obtained using XRD analysis. The multilayer thin film of BTO/BFO structures possessed enhanced ferroelectric and ferromagnetic properties, which is found to be increasing as the number of layers increases. The maximum values of P_s = 99.80 $\mu C/cm^2$ and M_s = 94.70 emu/cm^3 were obtained for the six-layer system prepared using the PLD technique. The six-layer PLD-grown PV cell upon irradiation with 405-nm wavelength light with 160 mW/cm^2 intensity, showed a large increase in photocurrent from 4.5×10^{-7}A to 3.84×10^{-4}A as compared to the PV cell grown using CSD. The obtained magnitudes of short-circuit photocurrent density (J_{sc}) and open circuit voltage (V_{oc}) were 0.384 mA/cm^2 and − 0.40 individually with 0.098% light-to-electricity conversion efficiency for a six-layer PLD-grown PV cell.

Key words: Ferroelectric, ferromagnetic, photovoltaic, multilayer, thin film

INTRODUCTION

Researchers worldwide are working very hard to find alternate options for the generation of sustainable energy to meet the expanding requirements for abundant energy and clean fuel resources.[1–5] For the last few decades, efforts have been continuously made to harness solar energy using silicon-based photovoltaic (PV) technology which is a substitute to the diminishing energy sources. Typically, the PV effect involves two processes, creation of electron-hole pairs as the electrical charge carriers, and formation of electric current due to the motion of separated electrons and holes. The internal electric field that splits the charge carrier prevails in really limited space charge region across p-n junction in the case of junction-based photovoltaic effect. The radiation-provoked charge bearers are swept away from the depletion width exclusive of internal field in the material extent.[6] Therefore, there is a limited charge transportation in the junction-based photovoltaics due to this process of diffusion. For Si, the junction barrier height is ordinarily less than 1 V which cannot be run over by the open circuit

photovoltage (V_{oc}).[6–8]. Moreover, a p–n junction is not a prerequisite for the photovoltaic effect. The photovoltaic effect can emerge from a diversity of other processes such as a built in potential[7] or spin polarization.[8] Another mechanism called the bulk photovoltaic effect (BPVE) came into the picture, in non-centro-symmetric materials (like ferroelectrics), which was in contrast to the traditional photovoltaic effect in semiconductors involving the junction effect[9]. Large photo-voltage, with photocurrent proportionate to the ferroelectric–polarization intensity and charge barrier segregation is an exclusive feature of this alluring bulk ferroelectric photovoltaic effect (BFPVE) phenomenon.[9] In BFPVE, the remnant polarization and the polarization-driven internal electric field prevails in the entire extent of the ferroelectric instead of the narrow interfacial depletion layer. Here, the charge transportation is not bounded by diffusion, and V_{oc} is not barred by the energy band gap[10,11]. Therefore, the photo-voltage obtained in this case is substantially greater than the E_g (band gap).[11] The ferroelectric photovoltaic effect (FE-PV) was primarily inspected in different ferroelectric materials including $BaTiO_3$,[12,13] $PbTiO_3$,[14] $Pb(Zr,Ti)O_3$,[15] and PLZT[16]. A brief summary of the photovoltaic application of ferroelectric material is presented in Table I.

Oxide materials are cheap, abundant, stable, highly light absorbing and their characteristics can be methodically integrated via element replacements, making them favorable for thin film ferroelectric photovoltaics.[9,17] High motivation was achieved because of the exceptionally high open circuit photo-voltage (in some cases, $V_{oc} > 10^2$ V), which is obtained when crystal was subjected to illumination.[18–22]

However, the light-to-electricity conversion efficiency (power conversion efficiency) of the bulk PV effect in ferroelectric thin film-based solar cells is reported to be significantly lower ($< 10^{-4}$) than that of silicon-based solar cells available in the market.[2,10] Moreover, the large energy band gap of ferroelectric materials allows strong absorption of light in the UV region only. Recently, a different mechanism for the ferroelectric photovoltaic phenomenon is proposed for BFO, where the observed high photovoltaic voltage is related to the domain wall mechanism in the ferroelectric material instead of the bulk which contributes substantial vision to the photovoltaic effect in BFO.[23–33] Yang et al. (2010) was able to achieve above band-gap photo-voltages.[31]

The output of the ferroelectric-based solar cell can be adjusted by different other means including magnetic, electrical and mechanical functionality.

Table I. Brief summary on photovoltaic study carried out on ferroelectric samples

S. No.	Sample type	Deposition technique	Light source	Important results	References
1.	BFO/SRO/(111) STO, (110) DSO	PLD	λ = 550 nm with (100 mW/cm^2)	J_{SC} = 13.4 μA/cm^2	Basu et al.[17]
2.	BFO/SRO/(001) STO	MOCVD	White light (285 mW/cm^2)	V_{OC} = 0.9 V J_{SC} = 1.5 mA/cm^2 η = 10%	Yang et al.[2]
3.	BFO/SRO/(001) STO	RF magnetron sputtering	Incident light (λ = 435 nm) with (750 mW/cm^2)	V_{OC} = 0.3 V η = 7 $\times$ 10^{-4}%	Ji et al.[9]
4.	BFO/SRO/(111), (100) STO	RF magnetron sputtering	λ = 435 nm with (20 mW/cm^2)	Five order large bulk photovoltaic tensor coefficient β_{22}	Ji et al.[18]
5.	BFO/(001) Nb-STO	Laser molecular-beam epitaxy	He-Cd laser (λ = 325 nm) and pulsed Nd:YAG laser (λ = 355 nm)	V_{OC} = 136 mV	Wang et al.[19]
6.	ITO/BFO ceramic/Au	Solid state reaction	Diode lasers (λ = 373, 532 nm)	J_{SC} = 1.2 μA/cm^2	Hung et al.[20]
7.	BFO/FTO	Modified CSD	Solar simulator (100 mW/cm^2)	J_{sc} = 0.13 $\times$ 10^{-3} A/cm^2 V_{oc} = 0.65 V η = 5.34$\times$10^{-3}%	Dong et al.[21]
8.	BFO/Pt/Ti/SiO$_2$/Si(100)	Sputtering	λ = 405 nm laser	J_{SC} = 11.7 μA/cm^2	Chang et al.[22]
9.	In$_2$O$_3$-SnO$_2$/ BiFe$_{0.6}$Sc$_{0.4}$O$_3$/ LaNiO$_3$ (ITO/ BFSO/LNO)	RF magnetron sputtering		BFSO film in a negatively poled state, efficiency is improved fivefold with an enhanced switchable V_{oc} up to 0.6 V	Fan et al.[23]

Comparison of Ferroelectric Photovoltaic Performance in BFO/BTO Multilayer Thin Film
Structure Fabricated Using CSD & PLD Techniques

1837

The foundation of strain management can be engaged for the engineering of materials [multilayers and superlattices (SLs)] with improved magnetoelectric (ME) properties. Towards this aspect, numerous multilayer structures encompassing alternating ferromagnetic and ferroelectric layers have recently been studied, including $Pb(Zr,Ti)O_3/CoFe_2O_4$,[32,33] $(Pr_{0.88}Ca_{0.15}MnO_3)/(Ba_{0.6}Sr_{0.4}TiO_3)$,[34] $CoFe_2O_4/BaTiO_3$,[35] $BiFeO_3/BaTiO_3$,[36] $BiFeO_3$ and $BiMnO_3$[37] and were found useful in observing the enhanced ME properties. Upon investigation of $BiFeO_3/BaTiO_3$ SLs, it was concluded that structures with less modulation periods exhibited higher magnetic polarization and ME effect owing to increment in respective interfaces.[36–39]

Usage of appropriate ferroelectric materials with limited band gap in the visible region are encouraging towards the potential application in innovative solar energy devices. The lower optical band gap (2.2–2.8 eV) of multiferroic $BiFeO_3$ (BFO) has attracted recent interest of the research community because of its co-existing ferroelectricity, ferromagnetism and ferroelasticity. The interaction between these ferroic orderings may be adopted to endow next-generation photovoltaic cells with an appended range of capabilities. The physical mechanism of the photovoltaic effect in the multiferroic BFO system is not completely understood yet. It is clearly evident from Table I that the ferroelectric photovoltaic phenomenon was detected in BFO in various forms including single crystal,[40] thin films[23] and ceramics.[24,41–44] It is evident that the thin films are highly useful over single crystal or ceramics towards the device applications, because the poling voltage necessary in thin films is significantly low. However, the main limitation while using BFO thin film towards the ferroelectric photovoltaics is high leakage current deteriorating its ferroic and thus, PV properties. Along with this, BTO is another attractive ferroelectric material useful towards energy and charge storage, memories etc. owing to its extra-ordinary dielectric, piezoelectric and ferroelectric characteristics.[45] Nonetheless, BTO has a wide band gap (~ 3.3 eV) and, therefore, its use in the visible region photovoltaics is not possible. Researchers are making continuous attempts to decrease the energy band gap of BTO preserving its valuable ferroelectric characteristics towards the photovoltaic application in the visible region[46].

Reportedly, multilayer thin film-based structures occupy remarkable ferroic properties in comparison to respective thin film materials such as large ferroelectric and magnetic polarization, large dielectric constant with comparatively low losses.[47] Also, various other researchers have made efforts to modify the structure of ferroelectric materials or utilize different patterns of photovoltaic cells to obtain the improved ferroelectric–photovoltaic response but they have not achieved much success.[41–43] Hence, by depositing BFO and BTO multilayer structures, enhanced ferroelectric properties in BFO along with a lower band gap of BTO can be achieved. There are several reports along with of BFO and BTO, where band-gap adjustments have been displayed by producing multilayered structures.[48,49] However, efforts have not been made to study the ferroelectric-based photovoltaic output of BFO/BTO thin film-based multilayer structures. Therefore, in this work, BFO/BTO thin film-based multilayer structures were deposited by chemical solution deposition (CSD) and its multiferroic characteristics have been inspected with focus on the ferroelectric photovoltaic applications.

The PV cell with six consecutive layers of BFO and BTO exhibited the improved PV response characteristics (V_{oc} = 1.806 V and J_{sc} = 17.76 μA/cm^2), in comparison to the other prepared multilayer PV cells. In order to further enhance the PV characteristics, it was important to improve the quality of BTO and BFO thin films. It has been reported that the multicomponent oxide thin films with superior quality can be easily fabricated using physical deposition techniques such as pulsed laser deposition (PLD). PLD is superior in stoichiometric composition of multicomponent oxide thin films with convoluted components, especially BFO which has high volatility of bismuth. Since composition is a key factor in determining the crystal structure and defect profile in the deposited films, PLD has attractive advantages which can be used to control the desirable quality and structure of BTO and BFO thin films by adjusting the substrate temperature, laser fluence, deposition rate and time.[50] PLD also extends flexibility towards depositing different multilayer heterostructures of oxide materials with even high melting point. Therefore, in the second part of the present work, the BFO/BTO thin film-based multilayer structures have been prepared by PLD on different substrates and their structural, electrical, ferroelectric and ferromagnetic characteristics were studied. Thus, the BFO/BTO structure fabricated using two different deposition techniques has been studied for the ferroelectric–photovoltaic application and discussed in detail.

In conclusion, in the present work, BFO/BTO thin film-based multilayer structures have been deposited using CSD and PLD and its multiferroic characteristics have been investigated with focus on the ferroelectric–photovoltaic applications.

EXPERIMENTAL PARTICULARS

Multilayer structures containing respective BFO and BTO layers were fabricated utilizing both PLD and CSD techniques. The number of constituent layers (BFO and BTO) was varied from two to seven while keeping the entire thickness of the structure at 350 nm.

Deposition of Multilayer BFO/BTO Structures by the PLD Technique

The ceramic targets of $BiFeO_3$ and $BaTiO_3$ of 1-inch diameter were made for growing respective thin films in the multilayer system. Conventional co-precipitation was employed to prepare the $BiFeO_3$ ceramic target with 20% surplus bismuth and stoichiometric $BaTiO_3$ target.[51] BFO and BTO thin films were fabricated by Nd:YAG pulsed laser with fourth harmonic (λ = 266 nm) using PLD. The PLD chamber is thoroughly cleaned and evacuated to a base pressure of about 1.33×10^{-5} kPa to remove any unwanted impurities that might contaminate the deposited thin films. The critical processing parameters for the deposition of thin film using PLD include gas pressure, substrate temperature, laser energy density, target to substrate distance and the repetition rate of the laser pulse. The deposition parameters used in the present work to deposit BFO and BTO layers are summarized elsewhere.[51,52]

Before multilayer structure fabrication, a platinum (Pt) metal thin layer of 70 nm thickness was deposited over the passivated Si (i.e. SiO_2/Si) substrate by E-beam evaporation; a buffer layer of Ti (20 nm) was deposited in situ over SiO_2/Si prior to Pt deposition to improve the adhesion of Pt on SiO_2/Si substrate.

Since film crystallinity is greatly affected by the kinetics of atomic arrangements on the substrate surface during film deposition, substrate temperature was kept fixed at 750°C. Multilayer structures deposited on platinum-coated passivated silicon (Pt/Ti/SiO_2/Si) substrate were used for electrical, ferroelectric and photovoltaic measurements in MFM configuration with Au circular dots (200 μm dia) as the top electrodes. The Au top electrode was deposited using thermal evaporation.

Multilayer structures deposited under similar growth conditions on fused quartz substrate were used for XRD and surface morphology studies while the magnetic properties were studied using the Si substrate.

Deposition of Multilayer BFO/BTO Structures by the CSD Technique

The multilayer structure of BFO and BTO were grown on different substrates including Pt/Si, fused quartz and Si. Barium acetate and titanium *n*-butoxide were dissolved in 2-methoxyethanol and acetic acid with 1 ml of acetylacetone to prepare the BTO precursor solution. Bismuth nitrate and iron nitrate were dissolved in 2-methoxyethanol and 1 ml acetic acid to prepare the BFO precursor solution. The prepared solutions were blended well to obtain the final respective homogenous solutions. Solution spin casting was done to fabricate the BFO/BTO thin film multilayer system containing interspersed layers of BFO and BTO assemblage onto Pt/Ti/SiO_2/Si substrate. The BTO thin film was fabricated on Pt-coated Si substrate as the starting layer with BFO thin film as next layer respectively to get the final BFO/BTO multilayer system.

The number of layers (consecutively BTO and BFO) were changed from two, four and six while maintaining BTO as the first layer [BFO/BTO/Pt/Ti/SiO_2/Si (two-layer system), BFO/BTO/BFO/BTO/Pt/Ti/SiO_2/Si (four-layer system), and so on. The final prepared samples were annealed at 700°C. Thickness of respective BFO and BTO layers in the multilayer system were kept equal with the total thickness of the system at 350 nm. Thus, BFO/BTO bilayer structure had 175 nm thin BFO as well as BTO thin films, 87 nm for a four-layer (BFO/BTO/BFO/BTO) structure, respectively, and so on. The effect of number of constituent layers (BFO and BTO) in the multilayer structures on structural, optical, electrical, ferroic and photovoltaic properties had been studied.

RESULTS AND DISCUSSION

Structural Analysis: X-ray Diffraction

Figure 1 shows the XRD (θ–2θ) diffraction patterns of the prepared six-layer BFO/BTO multilayer system using both CSD and PLD techniques fabricated on Pt/Ti/SiO_2/Si substrates. It is inferred from XRD graphs that multilayer structures prepared using both techniques are polycrystalline with pure perovskite structure of BTO and BFO confirming the formation of explicit phase with an absence of
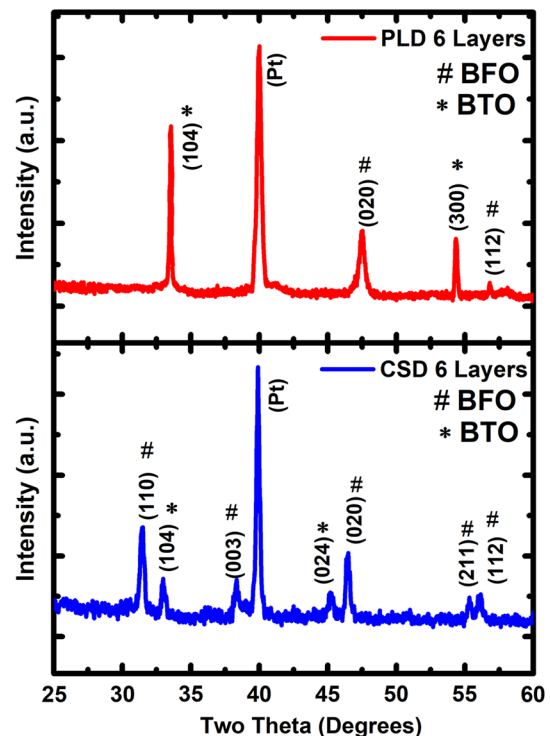

Fig. 1. XRD pattern of BFO/BTO multilayer systems with variation in constituent layers of BFO and BTO.

Comparison of Ferroelectric Photovoltaic Performance in BFO/BTO Multilayer Thin Film
Structure Fabricated Using CSD & PLD Techniques

1839

impurity (Fig. 1). The obtained XRD pattern conforms to respective tetragonal and rhombohedral structures of BTO and BFO. Le-Bail fitting was used to calculate the lattice parameters of BFO and BTO in the multilayer thin film structure. Table II summarizes the lattice parameters (a, c), c/a distortion ratio including induced strain along 'c' axis calculated from XRD data in BTO and BFO thin films, respectively, in the multilayer system. For comparison, data reported for bulk BTO and BFO has also been inserted in Table II. The variation in the lattice parameters, stress and c/a distortion (Table II) for multilayer structure prepared by PLD are similar to those observed earlier for the BFO/BTO multilayer structure prepared by CSD techniques and is attributed to the variation in the unit cell dimension of the constituent layers of BTO and BFO.[51,52] The lattice parameters values, a and c were approximated as 4.372 Å and 4.078 Å for BTO and 5.424 Å and 13.315 Å for BFO, respectively, for the six-layer BFO/BTO system prepared using CSD (Table II). However, the values of lattice specifications a and c were found to be 4.252 Å and 4.079 Å for BTO and 5.528 Å and 13.603 Å for BFO, respectively, for the six-layer BFO/BTO system for the PLD grown films. The obtained parameters are marginally inferior than the analogous bulk values for BFO and slightly higher in the case of BTO [JCPDS card No. 01-072-0138 and 01-072-2035],[51] indicating the presence of stress in the BFO/BTO multilayered structures. It can also be observed from Table III that the stress modulus in BTO and BFO thin films grown using PLD is very low as compared to CSD grown films, indicating the growth of crack free and uniform films using PLD. Moreover, the value of c/a distortion ratio is higher in PLD grown films resulting in better ferroelectric properties which is needed for higher photovoltaic response.

Optical Properties: UV–Visible Transmittance

The inset of Fig. 2 shows the optical transmittance graph of the six-layer BFO/BTO multilayer structures fabricated using CSD and PLD. Both multilayer structures are deposited over fused quartz substrate for the optical study and are found to be transparent (> 60%) over a wide range of wavelengths from 600 nm to 1100 nm (Fig. 2). A explicit and sharp absorption edge is observed at about 600 nm for BFO/BTO multilayer structures prepared using both techniques. The absorption edge in the PLD prepared multilayer structure is seen to be shifting towards lower wavelength as compared to that prepared using CSD. The obtained results clearly indicate that the prepared multilayer structures are suitable for the photovoltaic applications over the wavelength range 350–600 nm. Figure 2 also depicts Tauc plot of the fabricated six-layer BFO/BTO multilayer structures to estimate the band gap. It can be observed from Fig. 2 that the band gap of the PLD-grown BFO/BTO multilayer system is obtained as 2.67 eV which is lower than the band gap of the CSD-grown multilayer structure, i.e. 2.88 eV, resulting in higher photovoltaic response of PLD-grown six-layer BFO/BTO multilayer structure.

Ferroelectric Property: P-E Hysteresis Loop

Figure 3 shows the P–E hysteresis loops for the BFO/BTO multilayer structures prepared using CSD and PLD techniques, measured at 1 kHz frequency and room temperature under metal-ferroelectric-metal (MFM) capacitor configuration. It is seen from Fig. 3 that the fabricated multilayer systems exhibit explicit and saturated PE hysteresis curves. The obtained result indicates that all prepared multilayer structures possess good ferroelectric property. Figure 3 shows ferroelectric hysteresis loops for the CSD-prepared BFO/BTO multilayer sample and the PLD-prepared BFO/BTO multilayer sample, exhibiting a transition from square loop to classic hysteresis loop. Classic hysteresis loop exhibited by the PLD-grown sample manifest a substantial change in polarization after the applied electric field is around the value of coercive field, depicting that maximum domains are swapped with the applied field with an amount equal to the coercive field. However, the hysteresis loop around E_c is not completely at 90 degrees with the x-axis, implying that swapping of domain walls

Table II. Summarized Lattice parameters of the BTO and BFO layers in BFO/BTO multilayer systems fabricated by CSD and PLD techniques.

	BTO				BFO			
	Lattice parameter		Stress modulus (%)	c/a distortion ratio	Lattice parameter		Stress modulus (%)	c/a distortion ratio
	a (Å)	c (Å)			a (Å)	c (Å)		
Six-layer CSD	4.372	4.078	1.115	0.9327	5.424	13.315	3.980	2.4548
Six-layer PLD	4.252	4.079	1.140	0.9586	5.528	13.603	1.903	2.4607
Bulk	3.999	4.033	–	1.0085	5.876	13.867	–	2.3599

Table III. Comparison of photovoltaic properties of BFO/BTO multilayer structure prepared by PLD and CSD techniques

| Parameters	Six-layer BFO/BTO by PLD	Six-layer BFO/BTO by CSD
Saturation polarization (P_s)	99.80 μC/cm^2	95.85 μC/cm^2
Remnant polarization (P_r)	72.14 μC/cm^2	54.60 μC/cm^2
Saturation magnetization (M_s)	94.70 emu/cm^3	90.10 emu/cm^3
Remnant magnetization (M_r)	35.32 emu/cm^3	20.21 emu/cm^3
Open circuit voltage (V_{oc})	0.40 V	1.80 V
Short circuit current density (J_{sc})	132 μA/cm^2	17.73 μA/cm^2
On to Off ratio (I_{on}/I_{off})	8.53 $\times$ 10^3	2.95 $\times$ 10^3
Efficiency (η) (%)	0.098	0.067
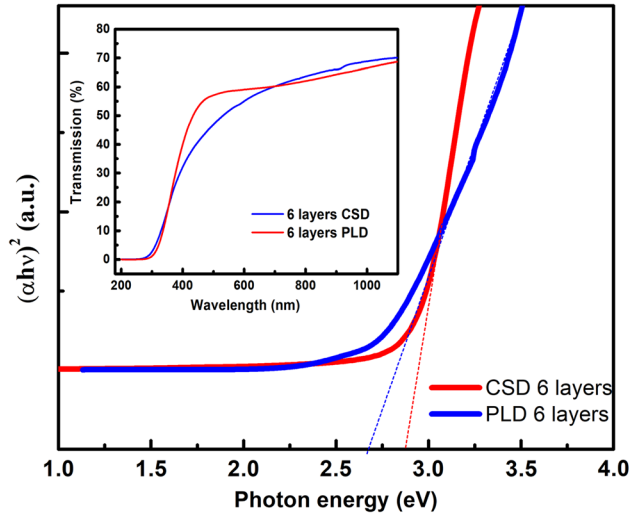
Fig. 2. UV–Visible Tauc plots of the BFO/BTO multilayer system fabricated over quartz substrates using CSD and PLD. Inset shows the transmission graphs of the BFO/BTO multilayer system.
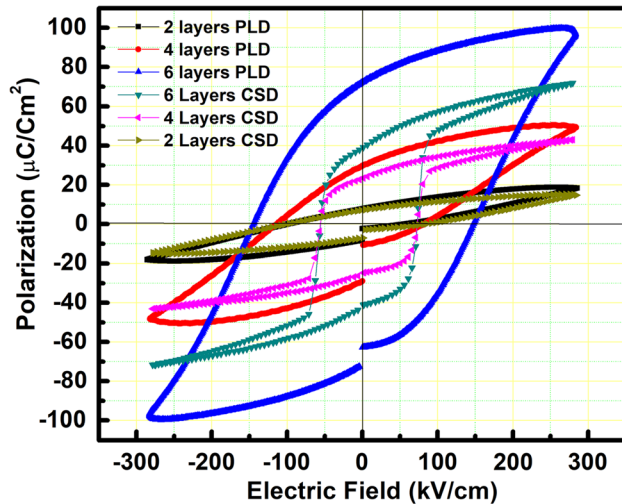

Fig. 3. Ferroelectric polarization versus applied electric field (P–E) curves obtained in the BFO/BTO multilayered structures with varying number of constituent layers.

is still present over the coercive field. This experience is associated with the clamping of domain walls, that may be induced electrically, mechanically, or chemically, whereas the CSD sample can be considered with larger grain without grain boundary. Thus, this clamping phenomenon due to the surrounding grains is absent in CSD samples[44].

The value of remnant polarization was seen to increase with an increase in the number of layers (Fig. 3) and exhibited a maximum value for both the CSD- and PLD-grown six-layer BFO/BTO structure. The observed improvement in remnant polarization of the BFO/BTO multilayer structure with advancing constituent layers may be attributed to several factors including the low leakage current, interface coupling between the constituent layers, the (110) preferred orientation of BFO crystallites and induced interfacial strain.[51–53] The observed magnitudes of remnant polarization ($2P_r$), saturation polarization (P_s) and coercive field ($2E_c$) for the fabricated multilayer systems are compiled in Table III and it can be inferred that the PLD-grown BFO/BTO multilayer thin film structures yield higher values of all ferroelectric parameters. This may result in higher photovoltaic response in PLD-grown BFO/BTO multilayer systems. The value of $2P_r$ of PLD-grown BFO/BTO multilayer structures increases from 19.33 μC/cm^2 to 108.12 μC/cm^2 (Table III) with an increase in respective layers from two (with each BFO and BTO layer of about 175 nm thickness) to six (with each layer of about 58 nm thickness), respectively, and the coercive field is also found to be increasing from 126.80 kV/cm to 195.22 kV/cm with number of stacking layers up to six layers. Gradual increase in the polarization with stacking layers may be attributed to the relative increase in interface coupling between layers (BTO and BFO). This is due to an increase in (110) preferred orientation of BFO crystallites and induced interfacial strain resulting into significant distortion in the ABO$_3$ perovskite structure of both BTO and BFO layers. The observed magnitudes of saturation polarization 23.77 μC/cm^2 to 95.85 μC/cm^2 for the two- and six-layered BFO/BTO systems, respectively, are found to be superior in comparison to previous reports for respective BTO and BFO thin films,[54] indicating the advantage of multilayer BFO/BTO structure over bare constituent layers.

Comparison of Ferroelectric Photovoltaic Performance in BFO/BTO Multilayer Thin Film Structure Fabricated Using CSD & PLD Techniques

1841

Magnetic Study

Figure 4 shows the magnetization versus magnetic field (M–H) hysteresis loops obtained at room temperature of the fabricated BFO/BTO thin film multilayer systems prepared using both PLD and CSD. Well-saturated M-H hysteresis graphs are obtained for all the BFO/BTO multilayer systems of total thickness 350 nm (Fig. 4). The saturation magnetization (M_s) for the BFO/BTO multilayer system is observed to gradually increase with an increase in the constituent layers of BFO and BTO while maintaining a constant total thickness at 350 nm (Fig. 4) for BFO/BTO multilayer structures prepared using both PLD and CSD. The values of saturation magnetization (M_s) obtained for the prepared multilayer BFO/BTO systems with a distinct number of layers are presented in Table III for comparison. The value of M_s obtained for the BFO/BTO multilayer system is higher in contrast to the corresponding values published for bare BFO thin films ($\sim$ 13 emu/cm^3) grown by PLD. The variation in the value of M_s obtained for the multilayer system as a function of the number of stacking layers is shown in Fig. 4. It can be inferred that the PLD-grown BFO/BTO multilayer structures produce higher values of all ferromagnetic parameters. This may be attributed to the lower stress obtained in PLD-grown BFO/BTO thin film multilayer structures. It may be seen that the M_s value gradually increases from 25.65 to 90.10 emu/cm^3 with increasing layers from two to six in the BFO/BTO multilayer system grown using PLD. The maximum value of M_s = 90.10 emu/cm^3 is obtained for the six-layer structure (Table III). This may be attributed to the fact that the thickness of constituent layers (BFO and BTO) gradually decreases from 175 nm to 58 nm for two- to six-layer structures. The thickness of constituent layers ($\sim$58 nm) for BFO/BTO multilayer structures with six layers

becomes comparable to the characteristic cycloid spin spiral modulation periodicity of 62 nm reported for BFO[53], and results in a higher value of M_s (Table III) in the present work. Such observation is found to be consistent with the other reports available in the literature[54–62]. As given in literature, coercive field (M_C) values depends on practical polarization switching affected by nucleation and growth of domains[54]. In an obliquely deposited ferromagnetic film, the coercive field increases sharply as the deposition angle becomes more and more tilted resulting in square hysteresis loop. Thus, PLD has an advantage over CSD to grow highly aligned thin films. Nevertheless, the magnetic characteristics of the BFO/BTO multilayers fabricated by PLD in the current article are superior in contrast to previous reports for the BTO/BFO multilayer structure fabricated by PLD[58,59]. The observed enhancement in the ferroelectric polarization along with the improvement in magnetization for the six-layer BFO/BTO structure, suggests a strong interface coupling between the constituent layers (BFO and BTO) and induced interfacial strain in the stacking layers.

Ferroelectric-Photovoltaic Studies

Figure 5 illustrates the comparison of current density–voltage (J–V) properties acquired for the six-layer BFO/BTO multilayer system fabricated using CSD and PLD techniques in dark and radiance conditions (λ = 405 nm). The J–V graph in radiance conditions (Fig. 5) showed a conventional ferroelectric photovoltaic phenomenon. The open-circuit voltage (V_{oc}) and short-circuit current density (J_{sc}) were approximated as $-$ 0.40 V and $-$ 1.80 V, 17.73 μA/cm^2 and 0.384 mA/cm^2, respectively, for PLD- and CSD-fabricated six-multilayer systems, respectively, as calculated using intercepts of the horizontal and the vertical axes (Fig. 5a and b). The values of various photovoltaic response parameters at zero bias for both multilayer systems are listed in Table III. It may also be noted from Table III that the magnitude of J_{sc} is much higher in the case of the PLD-grown BFO/BTO multilayer system as compared to that grown by CSD due to the superior ferroelectric properties in the PLD-grown BFO/BTO multilayer system.

From Fig. 5a it can be seen that the value of J_{sc} for PLD-grown BFO/BTO multilayer structure increases from 16 μA/cm^2 to 132 μA/cm^2 with increase in the number of layers from two to six. This enhancement in J_{sc} must be credited to high polarization intensity owing to improved interfusion strain in the six-layered BFO/BTO multilayer system fabricated using PLD. However, the obtained value of J_{sc} for the four-layered BFO/BTO multilayer system was low in comparison to the six-layered multilayer system because of its relatively lower polarization magnitude and higher leakage current density. Enhanced ($\sim$8.533 $\times$ 10^3) ON to
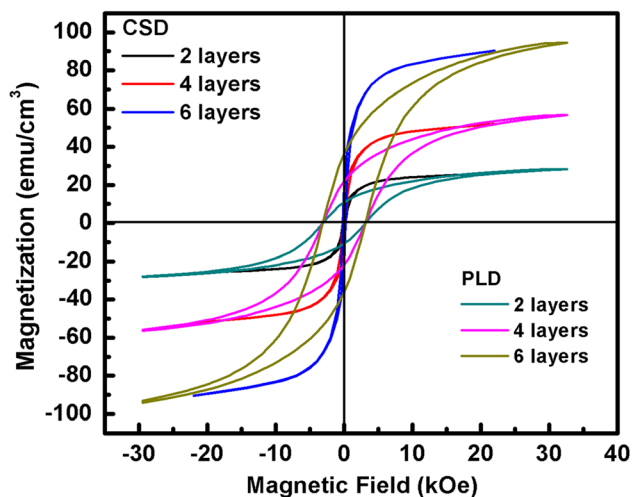

Fig. 4. Magnetization versus applied magnetic field (M–H) curves obtained for the BFO/BTO multilayered structures with varying number of constituent layers.
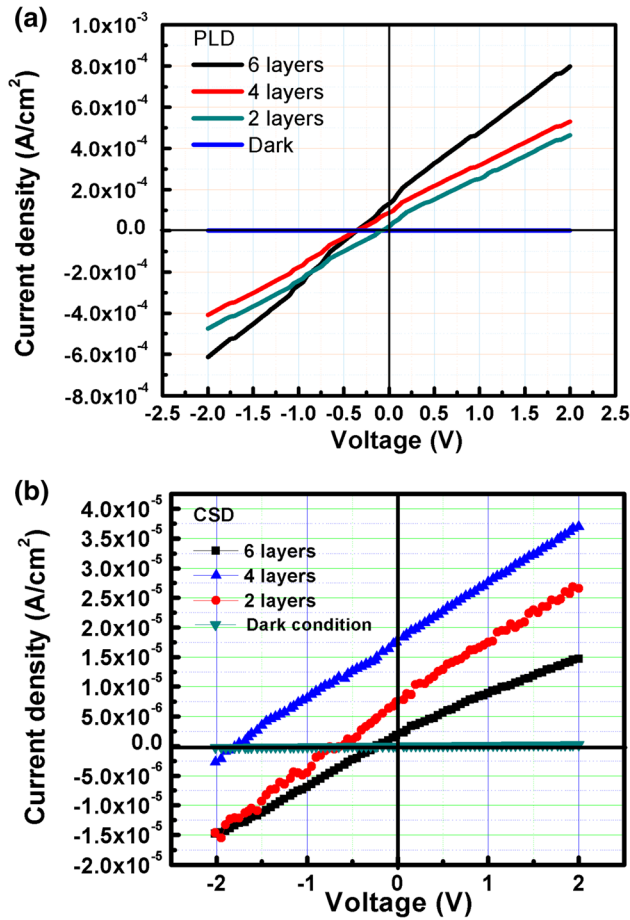
(a)

(b)

Fig. 5. (a) J–V plots obtained in fabricated multilayer BFO/BTO system deposited by PLD with two, four and six layers in dark and radiance conditions. (b) J–V plots obtained in the multilayer BFO/BTO system deposited by CSD with two, four and six layers in dark and radiance conditions.
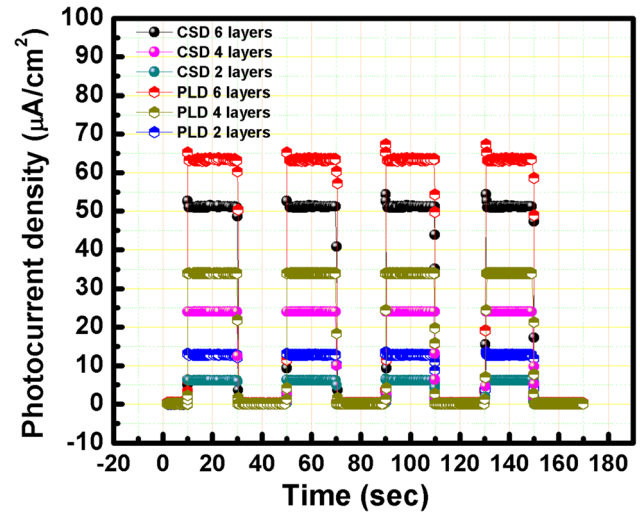

Fig. 6. Transient responses of short circuit current density of multilayer BFO/BTO structures having five and six layers at different radiance conditions.

OFF ratio was obtained for the PLD six-layer BFO/BTO multilayer system in comparison to the four-layer system. This was because of the origin and dispersion of additional light-caused charge barriers in radiance for the six-layer structure.

Figure 6 illustrates the transient response graphs of current density determined at zero applied voltage for two, four and six constituent layered BFO/BTO multilayer system fabricated using PLD and CSD in regular on and off radiance conditions (λ = 405 nm) at continuous 20-s intervals. From Fig. 6 it can be noted that the value of J_{sc} for the PLD-grown BFO/BTO multilayer system is higher than the J_{sc} for the CSD-grown BFO/BTO multilayer system. This observation is consistent with the enhanced ferroelectric polarization intensity owing to improved interfusion strain in the PLD fabricated BFO/BTO multilayer system as discussed in previous sections. When the radiance is switched off, the radiance generated current declines swiftly and achieves its initial value. Also, it is evident form the Fig. 6 that fabricated BFO/BTO multilayer system reciprocated immediately towards the incident

radiance and no deterioration in response could be seen in regular ON and OFF radiance conditions. Thus, it can be concluded that the ferroelectric domains inside the multilayer system switches swiftly. The observed outcome distinctly point towards the substantial utilization of fabricated multilayer BFO/BTO system for energy conservation.

Comparison Between CSD-Grown and PLD-Grown BFO/BTO Multilayer PV Cells

Table III tabulates the comparison of the six-layer BFO/BTO multilayer structure prepared by PLD with that of the multilayer structure prepared by CSD. The six-layer BFO/BTO structure prepared by PLD was identified to be the best suited for ferroelectric–photovoltaic applications with high I_{on}/I_{off} ratio and enhanced multiferroic properties as compared to the corresponding (six-layer) multilayer structure prepared by CSD.

It is interesting to note that a slight decrease in V_{oc} from 1.8 to 1.52 V was observed for the PLD-derived PV cell, but a significant increase in J_{sc} from 18 to 384 $\mu A/cm^2$ signifies the importance of the PV cell prepared by PLD. This was attributed to the formation of a sharp juncture amidst BFO and BTO layers by PLD in comparison to that of CSD, resulting in generation of maximum induced interface polarization due to large interfacial coupling. Furthermore, an increase in efficiency from 0.067% to 0.098% has been obtained for the PLD-derived PV cell which is ascribed to the efficient origination and dispersion of charge barriers.

SUMMARY

In the current article, multilayer BFO/BTO structures with two, four and six alternating layers were fabricated by both CSD and PLD and the effect of

Comparison of Ferroelectric Photovoltaic Performance in BFO/BTO Multilayer Thin Film Structure Fabricated Using CSD & PLD Techniques

1843

these two deposition techniques have been investigated towards the ferroelectric–photovoltaic properties. X-ray diffraction analysis confirms the production of perfect phase and polycrystalline structures of BTO and BFO thin films. Ferroelectric and ferromagnetic (multiferroic) characteristics of the multilayer BFO/BTO thin films improved with the advancement in respective BFO/BTO layers up to six layers. The leakage current density in the multilayer system exhibited a similar pattern holding minimal value 3.18 $\times 10^{-7}$ A/cm^2 for the six layered structure. The six-layer thin film multilayer structures exhibited an outstanding growth in current density from 4.50×10^{-7} A/cm^2 to 3.84×10^{-4} A/cm^2 upon radiance condition. The PLD prepared six-layer BFO/BTO system showed large value of V_{oc} = 0.40 V, $J_{ON/OFF}$ = 8.53 $\times 10^3$ and responsivity (R) = 2.40 mAW^{-1} owing to its enhanced ferroelectric properties associated with momentous juncture coupling among six respective interfaces of BFO and BTO. The relatively high efficiency (η = 0.098 %) estimated at 405 nm for the fabricated multilayer BFO/BTO PV system using the PLD technique features its achievable realistic utilization in energy harvesting and multifunctional systems.

ACKNOWLEDGEMENTS

FUNDING

CONFLICT OF INTEREST

Author Monika Tomar, Principal Investigator of the project, has received research grants from the Department of Science & Technology (DST). Authors Vinay Gupta and Anjali Sharma are Co-Principal Investigators of the project.

REFERENCES

1. B.T. Marquis, and J.F. Vetelino, *Sens. Act. B*, 2001, **77**, p 100–110.
2. S.Y. Yang, L.W. Martin, S.J. Byrnes, T.E. Conry, S.R. Basu, D. Paran, L. Reichertz, J. Ihlefeld, C. Adamo, A. Melville, Y.-H. Chu, C.-H. Yang, J.L. Musfeldt, D.G. Schlom, J.W. Ager III., and R. Ramesh, *Appl. Phys. Lett.*, 2009, **95**, p 062909.
3. J. Zhang, X. Su, M. Shen, Z. Dai, L. Zhang, X. He, W. Cheng, M. Cao, and G. Zou, *Nat. Sci. Rep.*, 2013, **3**, p 2109.
4. B. Chen, M. Li, Y. Liu, Z. Zuo, F. Zhuge, Q.F. Zhan, and R.W. Li, *Nanotechnology*, 2011, **22**, p 195201.
5. W. Cai, C. Fu, J. Gao, Q. Guo, X. Deng, and C. Zhang, *Phys. B*, 2011, **406**, p 3583.
6. M. Qin, K. Yao, and Y.C. Liang, *Appl. Phys. Lett.*, 2008, **93**, p 122904.
7. A. Shah, P. Torres, R. Tscharner, N. Wyrsch, and H. Keppner, *Photo. Tech.*, 1999, **285**, p 692.
8. P. Peumans, S. Uchida, and S.R. Forrest, *Nature*, 2003, **425**, p 158.
9. B.W. Ji, K. Yao, and Y.C. Liang, *Adv. Mater.*, 2010, **22**, p 1763.
10. A.M. Glass, D. von der Linde, and T.J. Negran, *Appl. Phys. Lett.*, 1974, **25**, p 233.
11. S.Y. Yang, J. Seidel, S.J. Byrnes, P. Shafer, C.H. Yang, M.D. Rossell, P. Yu, Y.H. Chu, J.F. Scott, J.W. Ager III., L.W. Martin, and R. Ramesh, *Nat. Nanotech.*, 2010, **5**, p 143.
12. A.G. Chynoweth, *Phys. Rev.*, 1956, **102**, p 705.
13. P.S. Brody, and F. Crowne, *J. Elect. Mater.*, 1975, **4**, p 955–961.
14. V.M. Fridkin, *Photoferroelectrics* Springer, New York, 1979.
15. A. Kholkin, O. Boiarkine, and N. Setter, *Appl. Phys. Lett.*, 1998, **72**, p 130.
16. M. Qin, K. Yaoa, Y.C. Liang, and S. Shannigrahi, *J. Appl. Phys.*, 2007, **101**, p 014104.
17. S.R. Basu, L.W. Martin, Y.H. Chu, M. Gajek, R. Ramesh, R.C. Rai, X. Xu, and J.L. Musfeldt, *Appl. Phys. Letts.*, 2008, **92**, p 091905.
18. W. Ji, K. Yao, and Y.C. Liang, *Phys. Rev. B*, 2011, **84**, p 094115.
19. W. Mao, Q. Yao, Y. Fan, Y. Wang, X. Wang, Y. Pu, and X. Li, *J. Alloys Comp*, 2019, **784**, p 117–124.
20. Y. Zhou, R. Zhang, Y. Fan, Z. Wang, W. Mao, J. Zhang, Y. Min, J. Yang, Y. Pu, and X. Li, *Solid State Commun.*, 2018, **270**, p 12–16.
21. R. Zhang, Y. Zhou, Y. Zhu, Y. Li, L. Chu, Y. Min, J. Zhang, J. Yang, and X. Li, *Mod. Phys. Lett. B*, 2017, **31**(32), p 1750304.
22. W. Zhang, X. Zhu, L. Wang, X. Xu, Q. Yao, W. Mao, and X. Li, *J. Supercond. Nov. Magn.*, 2017, **30**, p 3001–3005.
23. Y. Wang, *J. Appl. Phys.*, 2011, **109**, p 124105.
24. C.M. Hung, C.-S. Tu, W.D. Yen, L.S. Jou, M.-D. Jiang, and V.H. Schmidt, *J. Appl. Phys.*, 2012, **111**, p 07D912.
25. W. Dong, Y. Guo, G. Bing, L. Hongyan, H. Li, and L. Hezhou, *Mater. Lett.*, 2012, **88**, p 140–142.
26. H.W. Chang, F.T. Yuan, Y.C. Yu, P.C. Chen, C.R. Wang, C.S. Tu, and S.U. Jen, *J. Alloys Comp.*, 2013, **574**, p 402–406.
27. F. Fan, C. Changle, L. Bingcheng, and J. Kexin, *J. Appl. Phys.*, 2011, **109**, p 073716.
28. M. Alexe, and D. Hesse, *Nat. Commun.*, 2011, **2**, p 256.
29. A. Kumar, R.C. Rai, N.J. Podraza, S. Denev, M. Ramirez, Y.H. Chu, L.W. Martin, J. Ihlefeld, T. Heeg, J. Schubert, D.G. Schlom, J. Orenstein, R. Ramesh, R.W. Collins, J.L. Musfeldt, and V. Gopalan, *Appl. Phys. Lett.*, 2008, **92**, p 121915.
30. J. Allibe, K.B. Robin, E. Jacquet, I.C. Infante, S. Fusil, C. Carretero, J.L. Reverchon, B. Marcilhac, D. Crete, J.C. Mage, A. Barthelemy, and M. Bibes, *Appl. Phys. Lett.*, 2010, **96**, p 182902.
31. S.Y. Yang, J. Seidel, S.J. Byrnes, P. Shafer, C.H. Yang, M.D. Rossell, P. Yu, Y.H. Chu, J.F. Scott, J.W. Ager III., L.W. Martin, and R. Ramesh, *Nat. Nanotech.*, 2010, **5**, p 143–147.
32. N. Ortega, A. Kumar, R.S. Katiyar, and C. Rinaldi, *J. Mater. Sci.*, 2009, **44**, p 5127–5142.
33. J.P. Zhou, H. He, Z. Shi, and C.W. Nan, *Appl. Phys. Lett.*, 2006, **88**, p 013111.
34. P. Murugavel, M.P. Singh, W. Prellier, B. Mercey, C. Simon, and B. Raveau, *J. Appl. Phys.*, 2005, **97**, p 103914.
35. H. Zheng, J. Wang, S.E. Lofland, Z. Ma, L. Mohaddes-Ardabili, T. Zhao, L. Salamanca-Riba, S.R. Shinde, S.B. Ogale, F. Bai, D. Viehland, Y. Jia, D.G. Schlom, M. Wuttig, A. Roytburd, and R. Ramesh, *Nano. Sci.*, 2004, **303**, p 661–663.
36. H. Toupet, V.V. Shvartsman, F. Lemarrec, P. Borisov, W. Kleemann, and M. Karkut, *Integ. Ferro.*, 2008, **100**, p 165–176.
37. A. Chen, H. Zhou, Z. Bi, Y. Zhu, Z. Luo, A. Bayraktaroglu, J. Phillips, E.-M. Choi, J.L. MacManus-Driscoll, S.J. Pennycook, J. Narayan, Q. Jia, X. Zhang, and H. Wang, *Adv. Mater.*, 2013, **25**, p 1028.

38. V. Yang, K.M. Kim, J.Y. Lee, J. Zhu, and H.Y. Lee, *Int. Ferro.*, 2010, **113**, p 26–30.
39. G. Catalan, and J.F. Scott, *Adv. Mater.*, 2009, **21**, p 2463–2485.
40. M. Alexe, and D. Hesse, *Nat. Commun.*, 2011, **256**, p 1.
41. R.K. Katiyar, P. Misra, S. Sahoo, G. Morell, and R.S. Katiyar, *J. Alloys Comp.*, 2014, **609**, p 168–172.
42. H. Liu, K. Zhao, N. Zhou, H. Lu, M. He, Y. Huang, K.J. Jin, Y. Zhou, G. Yang, S. Zhao, A. Wang, and W. Leng, *Appl. Phys. Lett.*, 2008, **93**, p 171911.
43. Z. Fan, K. Yao, and J. Wang, *Appl. Phys. Lett.*, 2014, **105**, p 162903.
44. R. Yu, D.S. Shin, K. Jang, Y. Guo, H.M. Noh, B.K. Moon, B.C. Choi, J.H. Jeong, and S.S. Yi, *J. Am. Ceram. Soc.*, 2014, **97**(1), p 1–27.
45. W. Jiang, W. Cai, Z. Lin, and C. Fu, *Mater. Res. Bull.*, 2013, **48**, p 3092–3097.
46. R. Nechache, C. Harnagea, S. Li, L. Cardenas, W. Huang, J. Chakrabartty, and F. Rosei, *Nat. Photon.*, 2015, **9**, p 61–67.
47. N.M. Murari, A. Kumar, R. Thomas, and R.S. Katiyar, *Appl. Phys. Let.*, 2008, **92**, p 132904.
48. H.K. Yadav, K. Sreenivas, and V. Gupta, *Appl. Phys. Let.*, 2010, **96**, p 223507.
49. M. Lorenz, V. Lazenka, P. Schwinkendorf, F. Bern, M. Ziese, H. Modarresi, A. Volodin, M.J.V. Bael, K. Temst, A. Vantomme, and M. Grundmann, *J. Phys. D: Appl. Phys.*, 2014, **47**, p 135303.
50. K. Jiang, J.J. Zhu, J.D. Wu, J. Sun, Z.G. Hu, and J.H. Chu, *ACS Appl. Mater. Interfaces*, 2011, **3**, p 4844–4852.
51. S. Sharma, M. Tomar, A. Kumar, N.K. Puri, and V. Gupta, *J. Phys. Chem. Solids*, 2016, **93**, p 63–67.
52. S. Sharma, M. Tomar, A. Kumar, N.K. Puri, and V. Gupta, *Phys. B*, 2014, **448**, p 125–127. https://doi.org/10.1016/j.physb.2014.03.089.
53. S. Gupta, M. Tomar, and V. Gupta, *J. Appl. Phys.*, 2014, **115**, p 014102.
54. G. Qeemat, H. Wei, L. Yan, S. Rui, L. Na, Y. Xu, L. Yang, G.Z. Zhao, X. ZongKai, Z.X. Qun, and C.Z. Hua, *Chin. Phys. B*, 2018, **27**(9), p 097504.
55. M. Kumar, A. Srinivas, and S.V. Suryanarayana, *J. Appl. Phys.*, 2000, **87**, p 855–862.
56. J. Wu, W. John, X. Dingquan, and Z. Jianguo, *Appl. Surf. Sci.*, 2011, **257**, p 7226–7230.
57. K. Jiang, J.J. Zhu, J.D. Wu, J. Sun, Z.G. Hu, and J.H. Chu, *ACS Appl. Mater. Interfaces*, 2011, **3**, p 4844–4852.
58. P. Yang, K.M. Kim, J.Y. Lee, J. Zhu, and H.Y. Lee, *Int. Ferro.*, 2009, **113**, p 26–30.
59. Y.X. Yang, G.L. Yuan, Z.B. Yan, Y.J. Wang, X.B. Lu, and J.M. Liu, *Adv. Mater.*, 2017, **29**, p 1700425.
60. Z.A. Xiao, J.H. Zhao, C. Lu, Z.Y. Zhou, H. Wang, L. Zhang, J.J. Wang, X.Y. Li, K.Y. Wang, and Q.L. Zhao, *Appl. Phys. Lett.*, 2018, **113**, p 223501.
61. C.H. Yang, Y.J. Han, J. Qian, P.P. Lv, X.J. Lin, S.F. Huang, and Z.X. Cheng, *ACS Appl. Mater. Inter.*, 2019, **11**, p 12647–12655.
62. C.F. Ding, W.T. Hsiao, and H.T. Young, C.F. Ding, W.T. Hsiao, and H.T. Young, *Ceram. Int.*, 2019, **45**(13), p 16387–16398.